RESEARCH ARTICLE

WILEY

Supervised classification of landforms in Arctic mountains

Huw Thomas Mithan[1,3] 🔗 | Tristram Charles Hales[1] | Peter John Cleall[2]

[1] School of Earth and Ocean Sciences, Cardiff University, Cardiff, UK

[2] School of Engineering, Cardiff University, Cardiff, UK

[3] Department of Geography and Environmental Science, University of Dundee, Dundee, UK

Correspondence
 H. T. Mithan, School of Earth and Ocean Sciences, Cardiff University, Cardiff, UK.
Email: huwmithan@gmail.com

Abstract

Erosional and sediment fluxes from Arctic mountains are lower than for temperate mountain ranges due to the influence of permafrost on geomorphic processes. As permafrost extent declines in Arctic mountains, the spatial distribution of geomorphic processes and rates will change. Improved access to high-quality remotely sensed topographic data in the Arctic provides an opportunity to develop our understanding of the spatial distribution of Arctic geomorphological processes and landforms. Utilizing newly available Arctic digital topography data, we have developed a method for geomorphic mapping using a pixel-based linear discriminant analysis method that could be applied across Arctic mountains. We trained our classifier using landforms within the Adventdalen catchment in Svalbard and applied it to two adjacent catchments and one in Alaska. Slope gradient, elevation–relief ratio and landscape roughness distinguish landforms to a first order with >80% accuracy. Our simple classification system has a similar overall accuracy when compared across our field sites. The simplicity and robustness of our classification suggest that it is possible to use it to understand the distribution of Arctic mountain landforms using extant digital topography data and without specialized classifications. Our preliminary assessments of the distribution of geomorphic processes within these catchments demonstrate the importance of post-glacial hillslope processes in governing sediment movement in Arctic mountains.

KEYWORDS

Alaska, geomorphometry, linear discriminant analysis, periglacial landforms, supervised classification, Svalbard

1 | INTRODUCTION

Sediment fluxes from Arctic mountains are amongst the lowest on the planet,[1] despite having large stores of sediment[2] and enough topography to drive sediment transport. This anomalous observation has been ascribed to the role of permafrost in reducing erosion and sediment transport rates.[1] Permafrost distributions in Arctic mountains are particularly sensitive to changes in Earth's climate, as higher temperatures, changing precipitation patterns, and more frequent extremes of precipitation and temperature[3] can induce permafrost thaw and increase rates of surface processes.[3-5] As the climate warms, we would expect the spatial and temporal patterns of erosion and sediment transport from Arctic catchments to change. For example, weather extremes appear to drive more frequent active layer detachment slides that affect key areas of linear infrastructure in Arctic regions.[6] As climate drives differences in the distribution of Arctic

permafrost, it is important to understand how the spatial distribution of potentially hazardous surface processes (and their rates) may change.

Mapping of the distribution of geomorphic processes and landforms is not new in Arctic mountains. Since Rapp (1960)[7] first mapped Kärkevagge, there has been considerable effort to constrain the distribution of Arctic geomorphic processes and rates. At a landform scale, systematic mapping and measurement of process rates has occurred in blockfields,[8] solifluction,[9,10] and scree (talus) slopes.[11,12] Much of this effort has involved manual mapping, which remains the method that produces the most accurate maps, although the time-consuming nature of this method restricts its utility to local- and regional-scale maps. The reliance on expert interpretation subjects this method to varying degrees of accuracy.[13] Remotely sensed methods provide an alternative and there is a significant body of work dedicated to the study of geomorphometry as reviewed by Romstad and Etzelmüller (2012).[14] This work is supported by improvements in the quality of remotely sensed data that have allowed more detailed analysis into remote areas and at regional scales.[13,15–17] These automated classification methods allow for larger areas to be mapped more quickly while reducing human error (although introducing machine error), and facilitating

comparable results and model transferability.[13,18] At regional scales, topographic parameters derived from digital elevation models (DEMs) are shown to be one of the primary predictors of landforms in periglacial environments,[13,19,20] particularly in high-Arctic environments because of the low abundance of vegetation.[19] Statistical analyses of remotely sensed topographic, optical and/or climate data landform classifications[21] use a range of multivariate and simple statistical techniques including generalized linear methods such as linear discriminant analysis (LDA),[13,22] logistic regression,[17] and artificial neural networks.[13,23] Reported comparisons of different suites of statistical modeling suggest that simple models such as LDA and logistic regression perform equally when compared to more complex machine-learning techniques.[24,25] The inclusion of optical remotely sensed data or climate data can improve fine-scale differentiation of geomorphic features with similar topography but different levels of activity (such as differentiating active and less active talus sheets). However, due to the strongly variable nature of Arctic vegetation, optical solutions are difficult to translate across landscapes. Optical remote sensing may have more traction in vegetation-free areas, such as hyperspectral,[26] thermal inertia mapping[27] or texture filters applied to high-resolution optical imagery.[28] In addition, high-resolution cloud-free optical imagery and climatic data for remote

FIGURE 1 (a) Map of Svalbard with two of the three study sites: Endalen and Ringdalen. (b) Map of Alaska with the third study site: Saviukviayak. (c) View looking north-east down the Endalen valley (image taken by Huw Mithan) [Colour figure can be viewed at wileyonlinelibrary.com]

areas of the Arctic are difficult to obtain[29] whereas topographic data for the entire Arctic are readily accessible.[30] We develop a technically simple classification of geomorphic features that can be applied across the Arctic. The purpose of geomorphic classification is to improve our ability to understand, to a first order, the spatial distribution of important sources and sinks of sediment within mountainous Arctic catchments. To achieve this goal, our classification must pass two key tests: (a) that it can be implemented using regionally available digital terrain data, and (b) it must classify landforms that clearly relate to processes of either erosion or deposition in the current climate. For example, erosion of till or moraine by solifluction processes would be defined as a solifluction sheet. To achieve the balance of technical simplicity and geomorphic process focus, we settled on a pixel-based statistical landform classifier that uses LDA. We demonstrate the potential utility of this model for cross-Arctic mapping of landforms by comparing classifications in Svalbard and Alaska.

2 | STUDY AREAS

2.1 | Western Svalbard

We investigated two catchments in western Svalbard, Endalen and Ringdalen (Figure 1a). The study area is a high-Arctic semi-arid desert, with a mean annual temperature of −6.8°C and a mean annual precipitation of 190 mm (1961 to 1990, Svalbard Airport).[9] Permafrost is continuous outside of the glacier-covered areas and is typically 100 m thick in valley bottoms and 400–500 m thick at higher elevations.[31] The dominant geology is early Cretaceous to Eocene near-horizontally bedded sandstones, siltstones, shales and coal.[32] The landscape is mountainous with 400 m of relief. Summit areas are typically flat plateaus composed of blockfields and patterned ground. Frost-weathered sedimentary bedrock at plateau edges[33] leads downslope to steep planar (30°–40°) deposits of scree and debris fans. Shallow (5°-25°) concave slopes of solifluction sheets are found at the base of many hillslopes (Figure 1c). Valley floors contain braided river systems that deposit sediment at valley mouths to form alluvial fans. The areas around Endalen and Ringdalen have both seen extensive field investigations across a range of different geomorphic features, including studies of rockfall retreat,[12,34] debris flows/active layer detachment slides,[35] solifluction sheets/lobes,[9,36] and alluvial and colluvial deposits.[37]

2.2 | Brooks Range, Alaska

The Saviukviayak catchment forms in the eastern half of the Brooks Range (68.77°N, 147.48°W) of Alaska (Figure 1b). According to the nearest weather station, 190 km to the southeast at the Anaktuvuk Pass (68.14°N, 151.74°W), the annual mean temperatures are −8.3°C with a mean annual precipitation of 280 mm.[38] Bedrock is mainly chert and limestone that was uplifted, folded and faulted during the Cretaceous. The landscape is mountainous, with 600 m of

relief and a wide range of mountain landforms, and as such it is qualitatively similar to Endalen and Ringdalen, Svalbard. A braided river system, called Saviukviayak, traverses the valley with steep slopes rising from 845 to 1445 m where there are ridge summits. The Brooks

TABLE 1 Geometry of landforms used to train the classifier

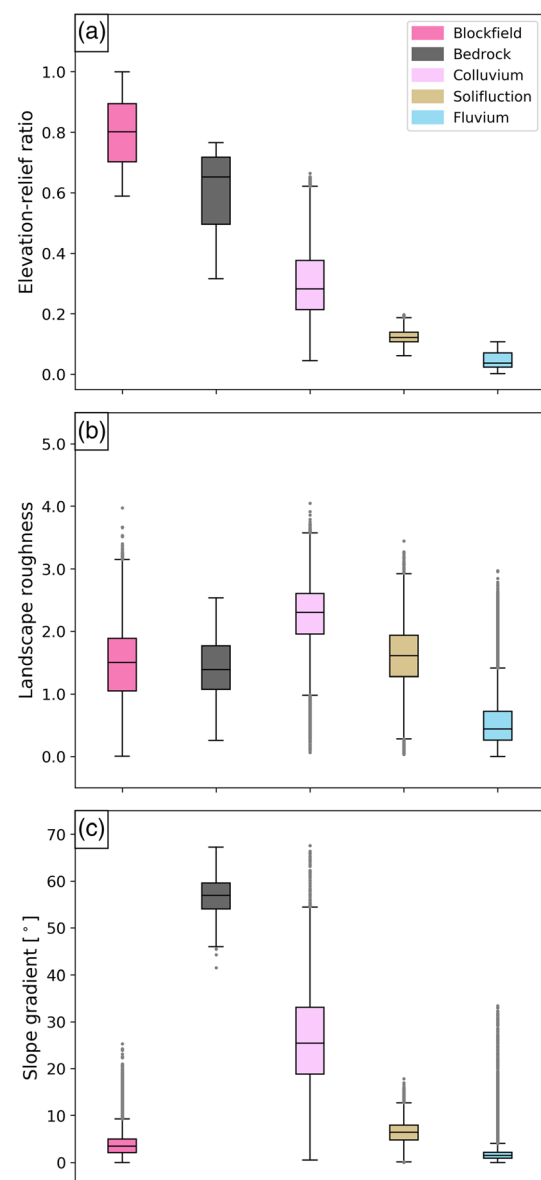| Adventdalen landforms	Number of polygons	Total area (km^2)
Blockfield	5	4.46
Bedrock	23	0.01
Colluvium	26	1.75
Solifluction	4	0.53
Fluvium	13	19.02

FIGURE 2 Topographic parameters for each landform used to train the classifier. (a) Elevation–relief ratio. (b) Landscape roughness. (c) Slope gradient [Colour figure can be viewed at wileyonlinelibrary.com]

Range was glaciated during the Pleistocene and since deglaciation most of it has been underlain by continuous permafrost. On the valley floor and on hillslopes, superficial deposits are either glacial drift and/or colluvium.[39]

3 | METHODS

3.1 | Geomorphology mapping

We created a geomorphological map using 5-m resolution satellite imagery of Endalen,[40] Ringdalen[40] and Saviukviayak.[41] Following the nomenclature of Tolgensbakk et al. (2000),[42] we mapped all non-glacial landforms as one of the following: blockfields, bedrock outcrop, colluvium (allochthonous material and scree slopes), solifluction sheets and fluvium (floodplain and alluvial fan material). Blockfields were flat areas found on summit plateaus with individual angular blocks observed in the satellite imagery. Bedrock outcrops tend to be found at the margins of summit plateaus bounded by scree slopes. In imagery, bedrock is darker in color and often contains significant shadow due to the steep nature of outcrops and low sun angle. Allochthonous material is defined simply as material that has moved downslope from its point of origin (such areas are generally termed as debris-mantled slopes), and we identified these regions to be in the transition zone from active (gray in imagery) to less active material (yellow-green in imagery). Tolgensbakk et al. (2000)[42] used this term to indicate material that was found on side slopes that could not obviously be tied to a specific landform or

process.[42] We have continued to use this definition. Scree (talus) slopes are planar or slightly fan-shaped, are non-vegetated, contain blocky material and are typically located mid-slope below exposures of bedrock. Solifluction sheets are found at the base of hillslopes, are vegetated and contain lobate deposits.[10] We identified floodplains based on their multiple weaving channels caused by braided rivers. The floodplain boundary sometimes included a steep ridge or bank. Alluvial fans are located at the exit of valleys and contain braided rivers and a distributary channel system. The lateral margins are defined by a change in color of the landform material and incised fluvial channels.

3.2 | Classifier development, training and testing

We trained an LDA classifier[43] using mapped landforms from Adventdalen (Table 1). LDA finds the best linear combination of topographic parameters that (a) maximize the distance between the means of two or more classes, while (b) minimizing the scatter around the mean within each class. LDA projects this information onto a new axis called linear discriminant 1 (LD1), linear discriminant 2 (LD2), etc., with LD1 representing the best linear combination of variables that fulfil (a) and (b). LDA has been widely and successfully applied to classify landforms, including periglacial applications.[22,24] We chose LDA because it is a simple tool for multi-class classification. It is possible to compare the linear relationship with expectations based on physical understanding of the processes governing each landform. For example, blockfields are known to form on summit plateaus with shallow slopes.
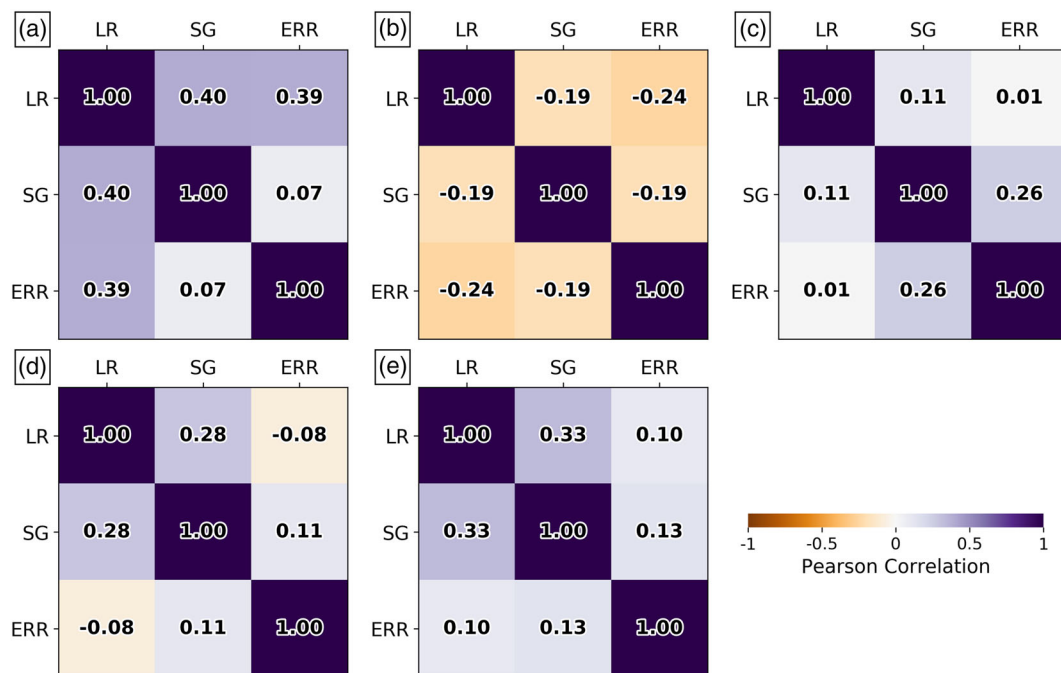

FIGURE 3 Pearson correlation between three topographic parameters for each landform. Landscape roughness (LR), slope gradient (SG), elevation–relief ratio (ERR). (a) Blockfield, (b) bedrock, (c) colluvium, (d) solifluction sheet and (e) fluvium [Colour figure can be viewed at wileyonlinelibrary.com]

During training of the model, we extracted the range of pixel values obtained from a 5-m photogrammetry-derived DEM for each mapped landform. We calculated ArcGIS-derived[44] slope aspect, slope gradient, planform curvature, profile curvature, total curvature, topographic wetness index,[45] topographic openness[46] and landscape roughness using a 3 × 3 pixel square window and the SR1 eigenvalue ratio.[47] We call SR1 the ratio of ln(S1/S2) where S1 is from McKean and Roering (2004).[47] Their study noted that the SR1 ratio can pick out other rough elements of the landscape such as roads, channels and bedrock outcrops. SR1 describes the tendency for vector data to be clustered such that braided rivers and alluvial fans have a greater landscape roughness or lower SR1 values because they are highly dissected with channels, and have high sediment loads of gravels, cobbles, boulders and sand banks. We used an elevation–relief ratio (ERR),[48] where ERR = $(x - x_{min})/(x_{max} - x_{min})$ for a 5-km-diameter moving window. The size of the window was consistent with other

measures of local relief[49] consistent with the typical width of a glacial valley.

We performed a recursive feature elimination analysis on our mapped landform dataset from Adventdalen to determine which topographic parameters contribute the most to the predictive power of the classifier. We found that the combination of ERR, landscape roughness and slope gradient returned the highest accuracy score during the recursive feature elimination analysis.

To assess the classifier's performance, we split the landform dataset into a 70% training set and a 30% testing set, and evaluated the classification using model accuracy metrics defined below. We repeated this train/test split procedure ten times on different segments of the landform dataset and took the average accuracy score. We used this test to ensure that the classifier did not perform differently after being trained on different segments of the landform dataset. Our classifier is trained using only 70% of the Adventdalen dataset, namely the 70%
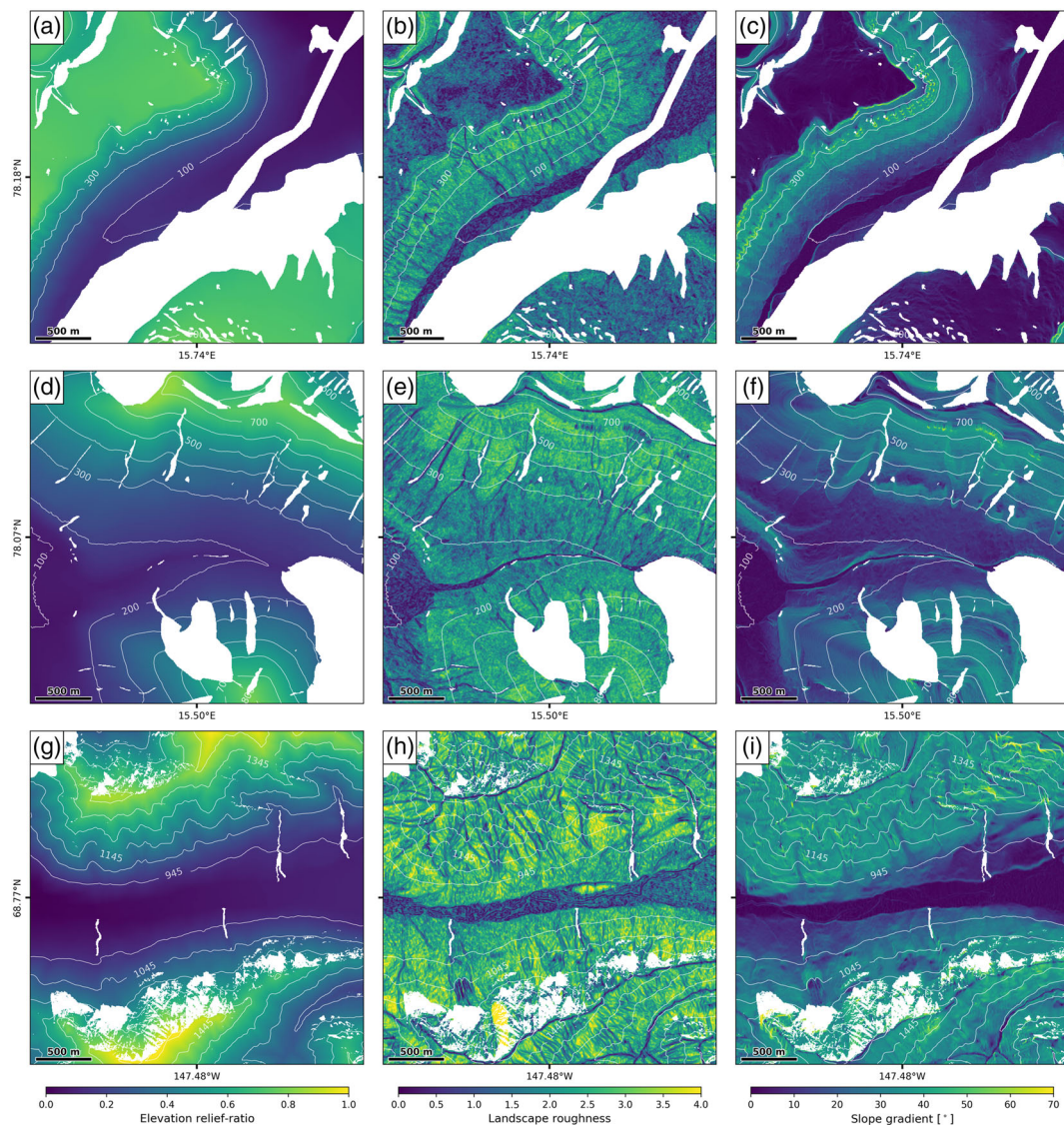

FIGURE 4 Elevation–relief ratio, landscape roughness and slope gradient map for each study site. (a–c) Endalen, (d–f) Ringdalen, (g–l) Saviukviayak. White areas represent regions with no data. Contours are in meters [Colour figure can be viewed at wileyonlinelibrary.com]

training set. From this point onward, we will call this our "trained classifier." Despite choosing a relatively small, but representative area ($n < 10$ for some features), the training and testing datasets were accurate at >80%, suggesting that these metrics capture these features well.

3.3 | Classifier application

We applied the trained classifier to the Endalen, Ringdalen and Saviukviayak catchments. We used DEMs of different sources to classify the remaining locations: a 5-m-resolution photogrammetry-derived DEM (Endalen and Ringdalen) and a 5-m synthetic aperture radar-derived (Saviukviayak) DEM.[50,51] Removal of anthropogenic infrastructure, water bodies, artefacts, pixels that were within the shadow shown in the satellite image, pixels that correspond to snow cover in the satellite image, glaciers and their features, and filled sinks in the raster surface fulfilled our final quality control step.

Assessment of classification quality was provided by three metrics: accuracy, recall and precision. Accuracy is the proportion of correct classifications (true positives [Tp] and true negatives [Tn]) from the overall number of cases (Tp, Tn, false positives [Fp] and false negatives [Fn], that is (Tp + Tn)/(Tp + Tn + Fp + Fn), thus giving an overall assessment of the classifier's performance. Recall is the proportion of correct positive classifications from the cases that are actually positive [Tp/(Tp + Fn)]. Precision is the proportion of correct positive classifications (true positives) from cases that are predicted as positive [Tp/(Tp + Fp)].

4 | RESULTS

4.1 | LDA classifier results

The LDA results show that more than 95% of the separation (the between-group variance divided by the within-group variance) between landforms is caused by a combination of the LD1 (64.94%) and LD2 (34.77%) axes. ERR controls 98.87% of the separation between landforms along the LD1 axis. Along the LD2 axis, slope gradient (11.47%) and landscape roughness (6.24%) have a greater influence but ERR remains dominant (82.29%). These results demonstrate that a considerable amount of the predictive power of the model lies with a small number of variables, ERR, slope gradient and landscape roughness. ERR and slope gradient are the strongest landform separators when used together.

4.2 | Landform topography and topographic metrics

Summit plateau blockfields were distinguishable as features of low slope gradient (average value of 3.8°) located in the higher parts of the landscape (average ERR of 0.80), with an average landscape roughness of 1.45. Bedrock is also found at higher elevations (average ERR of 0.59) on very steep slopes (average value of 56.8°) with average landscape roughness values of hillslopes (average ERR of

0.12) with low slopes (average value of 6.43°) and a landscape roughness of 1.58. Colluvium is modeled to be lower on the hillslope (average ERR of 0.3); however, with a standard deviation of 0.12 it does overlap with the ERR of bedrock. The average slope gradient for colluvium is 25.8° but these slopes are the smoothest of all landforms with an average landscape roughness value of 2.25. On the valley floor are the fluvial deposits with an average ERR of 0.04, the lowest average slope gradient of 1.7° and it is the roughest part of the landscape at 0.53 (Figure 2).

For each landform we used a Pearson correlation test to determine the correlation between topographic parameters (Figure 3). The strength of correlations between topographic parameters depends on landform type. Strong positive correlations occur between slope gradient/landscape roughness and ERR/slope gradient. The weakest correlations occur between ERR and landscape roughness. An exception is with bedrock where there are negative correlations between topographic parameters (Figure 3). A series of topographic maps for each study area (Endalen, Ringdalen and Saviukviayak) demonstrate
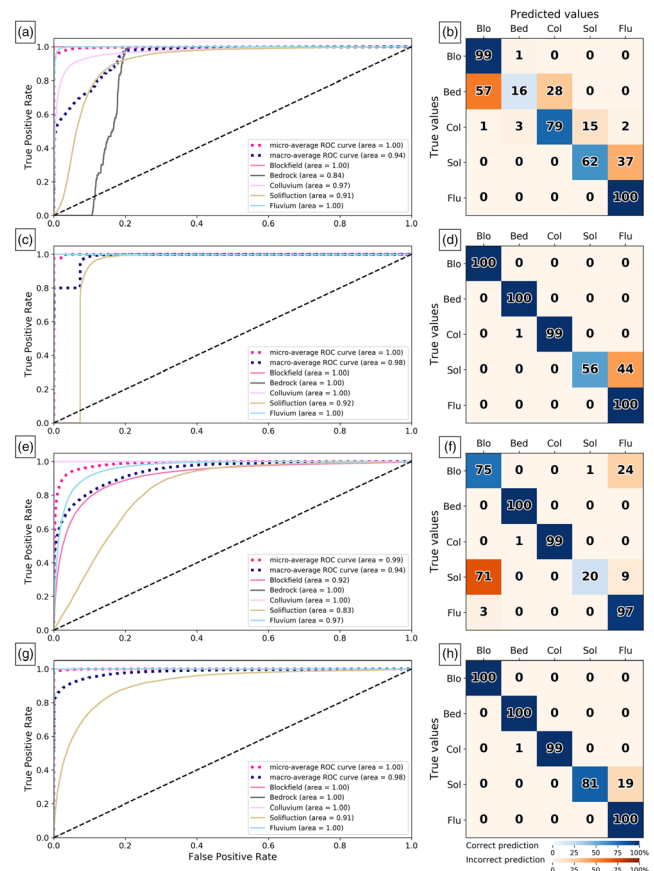

FIGURE 5 Area under the receiver operating characteristics curve (AUROC) when using a combination of topographic parameters to train the classifier. The plots on the right-hand side are confusion matrices. (a,b) Elevation–relief ratio and landscape roughness. (c,d) Elevation–relief ratio and slope gradient. (e,f) Landscape roughness and slope gradient. (g,h) Elevation–relief ratio, landscape roughness and slope gradient. Blockfield (Blo), bedrock (Bed), colluvium (Col), solifluction (Sol), fluvium (Flu). [Colour figure can be viewed at wileyonlinelibrary.com]

that topography is rougher (low value) on the summits and valley bottoms while slope gradients are steepest on the valley sides (Figure 4).

4.3 | Classifier internal testing

Initial internal testing of the model, with a 70% training and 30% test dataset split, produced a mean accuracy score of 99.51%. In general, recall and precision data demonstrate that reductions in accuracy are related to the misclassification of geomorphological units with similar surface topographies (e.g., solifluction sheets and fluvium). The model performs best when predicting blockfields (100% recall and 100% precision) and colluvium (100% recall and precision 99%). Solifluction sheets were also accurately identified (recall of 98%, precision of 81%). The most common misidentification was bedrock with a recall of 47%, where the other 53% is misclassified as colluvium. However, bedrock's precision is 100%, suggesting that of all the pixels it classified as bedrock 100% were classified correctly.

Our receiver operating characteristic (ROC) analysis on the training dataset shows that a combination of ERR, slope gradient and landscape roughness produces the highest area under the curve (Figure 5).

4.4 | Classifier implementation: Endalen

The classified map for a 10-km^2 area of Endalen (Figure 6d) has an overall accuracy of 88.91%. The confusion matrix (Figure 6a,d) demonstrates the success of the classification scheme in identifying the spatial distribution of landforms within these areas (Figure 6a). Occupying the flat plateaus of Endalen are blockfields, and this is the most extensive landform covering 38.86% of Endalen (Figure 7). Bedrock is modeled at the plateau edge, contouring the top of the hillslopes but also 100 m downslope from the plateau edge (Figure 6d). Bedrock covers the smallest area of 1.57% (Figure 7b). The mid-slopes are dominated by colluvium, which comprises the second largest landform (29.66%) of the study area. Its upslope boundary is defined by the plateau edge, bounding solifluction sheets at its downslope margin
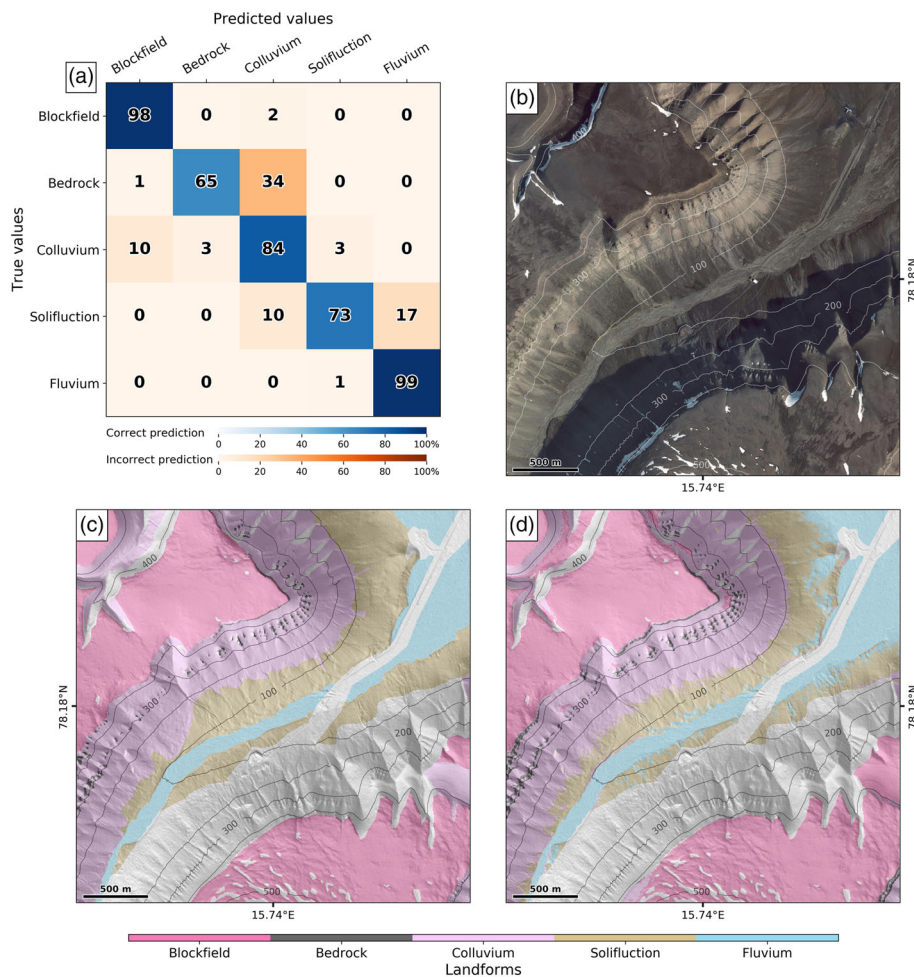

FIGURE 6 Endalen. (a) Confusion matrix comparing our geomorphology map (true values) to the classifier's map (predicted values) (%). (b) Satellite image of Endalen. (c) Our geomorphology map. (d) The classifier's geomorphology map. All images are underlain with a hillshade which may cause shading of the color schemes. Gray areas are regions of no data, which show the underlying hillshade. Contours are in meters [Colour figure can be viewed at wileyonlinelibrary.com]
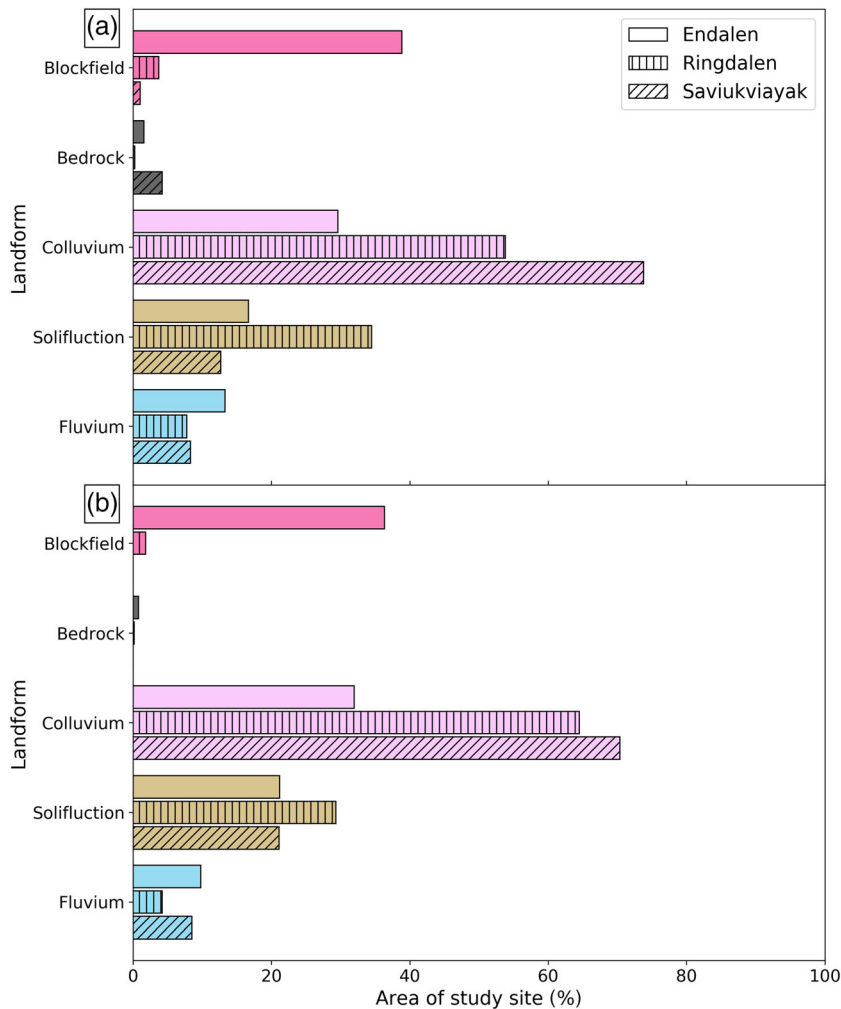
FIGURE 7 Bar chart showing the area occupied by each landform within all three study sites (excluding regions of no data). (a) Area of landforms in our map. (b) Area of landforms in the classifier's map [Colour figure can be viewed at wileyonlinelibrary.com]

(Figure 8). Solifluction sheets occupy 16.69% of the area, and represent the third most extensive landform. The downslope boundary of solifluction sheets borders the braided river and alluvial fan. Solifluction sheets are most extensive at the mouth of the valley (Figure 6d). Areas of solifluction sheets adjacent to the center of the valley contain pixels classified as alluvial fan. The extent of this increases toward the north-east. In the center, running from the south-west to north-east, is a mixture of pixels classified primarily as braided river, but some are incoherent clusters of alluvial fan material (Figure 3d).

4.5 | Classifier implementation: Ringdalen

The classified map for Ringdalen had an overall accuracy of 80.15% (Figure 9). Blockfields and flat plateaus are less dominant compared to Endalen, occupying 3.74% of Ringdalen (Figure 7b). The occurrence of bedrock is restricted to the top of cirques in the north-east and small ridges 500 m to the west. Colluvium dominates the landscape, occupying 53.62% of Ringdalen, and is extensive on north- and south-facing slope. Unlike in Endalen, colluvium in Ringdalen does not reach the valley floor. Solifluction sheets are the most extensive

landform (34.64%), in contrast to the other study sites. The classifier predicts solifluction sheets will occupy the lower half of the hillslopes in the center of Ringdalen and less in the south. Clusters of fluvium-classified pixels are found on the mid- to lower reaches of the soliflucting material. These clusters become denser at the mouth of Ringdalen. Patches of solifluction sheet occupy relatively flat sections of hillslope in the center north.

4.6 | Classifier implementation: Saviukviayak

The accuracy of the LDA model trained in Svalbard and applied to the Brooks Range is 81.54% (Figure 10). An interesting result of the classifier was the identification of blockfields (1.08% of the area), which we did not observe from our geomorphological mapping using satellite imagery. Upon re-analysis of the imagery it is evident that a flat plateau exists at the top of the narrow ridgeline. Colluvium occupies 73.02% (Figure 7b) of the study area, the largest proportion when compared to our sites on Svalbard. Bedrock is confined to the mid- and upper slopes, primarily north-facing slopes, and covering a relatively large area of 6.34% compared to our sites on Svalbard. Solifluction sheets (11.87% of area) dominate the lower slopes,
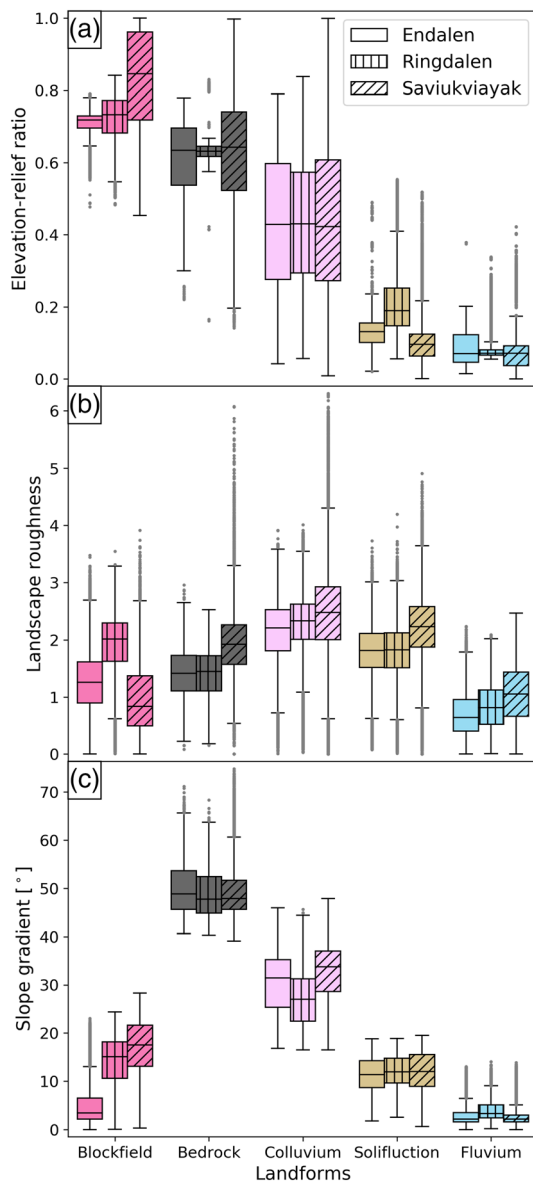
FIGURE 8 Topographic parameters of each landform from the classifier's map. (a) Elevation–relief ratio. (b) Landscape roughness. (c) Slope gradient [Colour figure can be viewed at wileyonlinelibrary.com]

particularly on south-west and north-east sides of the valley. Some solifluction sheets occur on south-facing slopes in a small valley in the south-east. Alluvium occupies the valley floor and on soliflucting slopes to the west. Interestingly, to the south-east the classifier identifies a region of alluvium on the floor of a small valley which we did not observe during mapping.

5 | DISCUSSION

We have developed a technically simple classification of geomorphic features that relate to processes of either erosion or deposition in the current climate and can be applied across Arctic permafrost.

Technically simple methods for classifying landscapes were originally developed for implementation using contour maps of topography.[49,52,53] Our model uses a three-parameter LDA chosen on the basis of a recursive elimination. Although we have achieved technical simplicity with our classification, there are questions as to whether our classification is too simplistic, particularly as there are alternative methods that include object-oriented[18] (rather than pixel-based) classification and those that incorporate readily available optical remote sensing data.[28]

Our pixel-based classification is strongest where the landform shape is simple and separated by clear breaks in slope gradient, ERR or landscape roughness (Figure 8). Hence, the classifier does best at determining blockfields, solifluction sheets and bedrock outcrops. Where topography is complex, the classifier does not perform well, such as the separation of alluvial fan and braided river floodplains or when a landform contains pixels that are close to a boundary (Figure 8). Falsely positive classified pixels arise because pixels inside a soliflucting landform are classified as floodplain. This occurs because pixel-based classifications form clusters of pixels with similar topographic parameters, resulting in dispersed classifications called the "salt and pepper effect."[54] If we restrict ourselves to topographic data, it might be possible to improve our topographic analysis by including a combination of topographically derived hydrology and pixel-based morphology. Recently, these methods have been useful in determining the upper limit of the channel network,[55,56] delineating floodplains,[57] or zero-order drainage basins.[58] By limiting ourselves to available >20-m-resolution topography, we are working at the limit of most process-based methods for topographic analysis.[59] We experimented with the inclusion of hydrologic parameters within our classifications, and found the extensive summit plateaus and planar side slopes in our field area led to anomalous positioning of channels relative to mapped channels. Alternatively, simple landform classifications using a small number of parameters have been used generically to distinguish areas by shape (rather than process).[60] These methods have proven extremely useful for landscape ecology and for regional- or continental-scale mapping. Yet, their deliberately generic nature does not allow for a simple relationship to geomorphic process.

Object-oriented landform classifiers have shown considerable promise as potential methods for identifying landforms.[18] Object-oriented analysis segments landscapes by grouping pixels into areas of consistent morphology that are separated by boundaries.[18] The essential difference between this and pixel-based methods is that context, landform shape and geometric signature can be accounted for in defining a landform.[61] Currently, object-oriented landform segmentation methods, for example geomorphon analysis[62] or elementary forms,[61] have been applied relatively locally at a catchment or smaller scale, or applied generically (i.e., identifying form only rather than form and process) across large areas. There is considerable discussion within the literature about the role of spatial scale, particularly the potential desire to create multi-scale object-oriented landform analysis,[63] and this has been resolved through, for example, hierarchical algorithms.[54] The issue of scale in this context reflects a
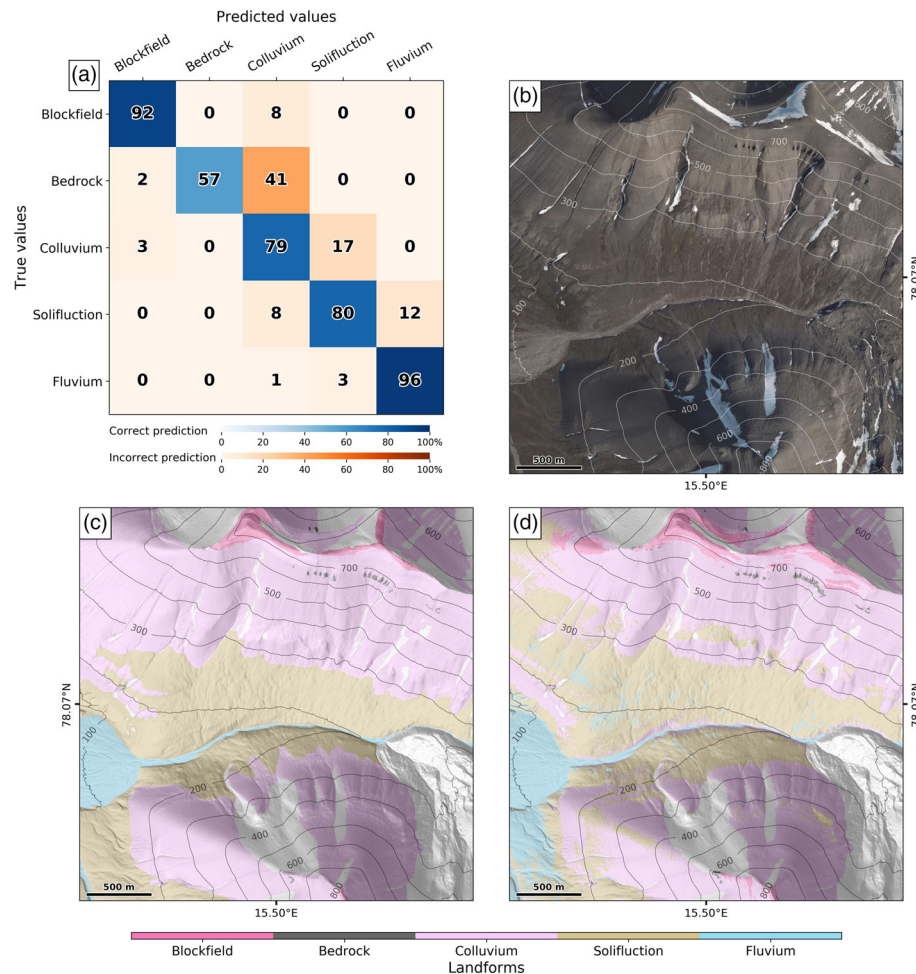
FIGURE 9 Ringdalen. (a) Confusion matrix comparing our geomorphology map (true values) to the classifier's map (predicted values) (%). (b) Satellite image of Ringdalen. (c) Our geomorphology map. (d) The classifier's geomorphology map. All images are underlain with a hillshade which may cause shading of the color schemes. Gray areas are regions of no data, which show the underlying hillshade. Contours are in meters [Colour figure can be viewed at wileyonlinelibrary.com]

debate on the scale at which different geomorphic processes act. This debate is well exemplified by the curvature scaling in soil-mantled landscapes that reflects the transition from pit and mound topography to hillslope diffusion.[64] Given the challenges with the implementation of these methods across wide spatial scales, we adopted the simpler, more parsimonious pixel-based characterization of landscape form.

Arctic landform classification has often included a combination of digital topography and optical remote sensing analysis. Spectral ratios that identify vegetation have been included in classifications of differential landforms with similar topographies.[28,54] The strength of this process is that it strongly differentiates landform disturbance rate, such that more active landforms cannot grow significant vegetation. In our field area, areas mapped as allochthonous slopes cannot be differentiated from scree slopes using topographic data alone. Instead, during the manual mapping of these landforms, they are differentiated using the total amount of vegetation. As a significant vegetation cover suggests inactivity at a decadal to centennial timescale for rockfall, a process with a strong stochastic component,

the presence or absence of vegetation does not necessarily improve our understanding of the underlying geomorphic process. As such, we do not view the inclusion of remotely sensed optical data as improving the effectiveness of our classification. Alternative remotely sensed analyses, such as hyperspectral analysis and thermal imagery,[32] had similar issues. In summary, our classification manages to maintain technical simplicity, while moving from a focus on generic landforms to a more process-oriented geomorphic classification of Arctic landforms.

Finally, we examined the uncertainty in our analysis formally using accuracy, recall and precision metrics. We trained the classifier on landforms in a single catchment, then applied the trained classifier, without recalibration onto the other locations. The overall accuracy score for the Ringdalen (80.91%) and Brook's Range (81.54%) is slightly lower than for the training site in Endalen (88.91%), but it remains high, suggesting that the uncertainty in parameter values between locations is relatively small. Internally, the major loss in precision and recall is where we have two landforms of similar origin, such as scree slopes and allochthonous slopes. As a first-order
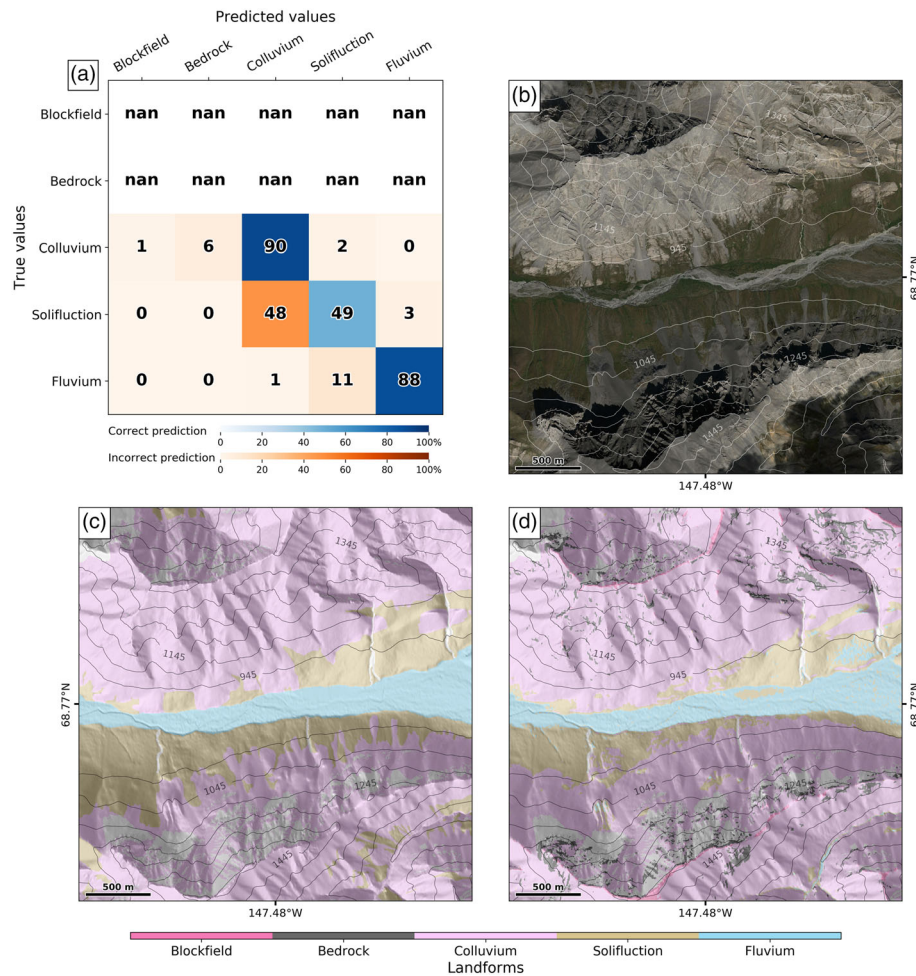
FIGURE 10 Saviukviayak. (a) Confusion matrix comparing our geomorphology map (true values) to the classifier's map (predicted values) (%). "nan" represents no data meaning that these landforms were not mapped by us. (b) Satellite image of Saviukviayak. (c) Our geomorphology map. (d) The classifier's geomorphology map. All images are underlain with a hillshade which may cause shading of the color schemes. Gray areas are regions of no data, which show the underlying hillshade. Contours are in meters [Colour figure can be viewed at wileyonlinelibrary.com]

methodology, these differences in classification suggest that methodological uncertainty outweighs the spatial uncertainties associated with applying the same classification to different geographical locations. Hence, we show that our simple classification provides a tool for the rapid mapping of landforms in Arctic mountains.

5.1 | Relationship between form and process

We sought to create a classification that reflected the underlying geomorphic processes governing the spatial distribution of landforms across Arctic Mountains. The three-parameter model does appear to separate major process transitions well. The slope gradient parameter separates steep bedrock from slopes that accumulate sediment close to their angle of repose (scree-like landforms), creep-dominated landforms (e.g., solifluction sheets) and fluvial landforms. Landscape roughness is useful for classifying bedrock, particularly within the smooth sedimentary landforms that surround it.[65] ERR is effective at identifying blockfields and fluvial systems that occur

at the highest and lowest parts of the topography, respectively. Supporting the utility of this application are our estimates of accuracy, precision and recall that generally show a high degree of statistical correlation. With the caveat that we classified only three Arctic catchments, our classifier can provide some insight into the spatial extent of landforms in mountainous permafrost environments. Blockfields are extensive on the plateaus above Endalen and represent either the upper altitudinal limit of glacially eroded terrain or their preservation under cold-based ice during the Last Glacial Maximum. The lack of extensive blockfields in Ringdalen and Saviukviayak may be a product of the bedrock structural geology and/or erosional history. There is considerably more bedrock found in our Alaska site than in Svalbard. The presence of bedrock outcrops reflects parts of the landscape where the weathering rate is lower than the erosion rate.[65,66] Hence, areas that have been recently glaciated or are steeper (due to tectonic or lithologic controls) are likely to be bedrock-dominated. Both the Brooks Range and Svalbard are tectonically inactive, suggesting a possible lithologic control on bedrock outcrop distribution. However, this could be

because both regions have been recently glaciated.[67] Vertical bedrock outcrops were challenging to map from satellite imagery, and the low recall and high precision of bedrock in our study sites suggests that our topographic methodology may be better at identifying bedrock outcrops than satellite mapping. Bedrock that is <10 m^2 is challenging to identify with relatively low-resolution satellite imagery, where shadows cast by mountain summits or steep bedrock faces hide landform boundaries. The small bedrock source area to large depositional landform area in Endalen and Ringdalen indicates that current erosional activity is low.

Solifluction sheets are extensive at shallow slope gradients.[13,17,68] We demonstrate that solifluction sheets are a common occurrence at the base of hillslopes. First, solifluction sheets occurs where soil is frost-susceptible, enhancing the development of ice lenses, which facilitates two fundamental processes: frost-heaving and gelifluction.[69] In Endalen, for example, the weathering of bedrock on the valley slopes is thought to produce frost-susceptible soils.[9] This material accumulates at the base of the hillslope by processes such as rill erosion, avalanching or cornice collapses.[70,71] Second, sufficient moisture is needed to feed the growth of ice lenses during autumn freeze-back, driving the frost-heaving component of solifluction. The base of these hillslopes has shallow slope gradients, where water from hillslope runoff, melting snow or thawing ice lenses accumulate. This excess saturates the soil, driving the gelifluction component of solifluction during spring thaw.[72] This therefore reduces soil shear strength, allowing it to deform downslope under its own weight. Finally, slope gradient must be steep enough to initiate downslope self-weight shear stresses but not too steep as this can cause failure along a shear plane or generate a debris flow.[73]

Colluvium occupies the greatest areal extent for Ringdalen (53.8%) and Saviukviayak (73.8%), while this landform is second only to blockfields in Endalen (29.4%). The dominance of colluvium and a low areal extent of bedrock outcrops (<5%) suggests that sediment accumulates and remains on Arctic hillslopes. This indicates that the degree of coupling from hillslope to channels, termed connectivity,[74] is low in our study areas. This is also evident across the Arctic because sediment yield from Arctic rivers is low when compared to their temperate counterparts.[1] Sediment production and transport are negatively impacted by low temperatures in the Arctic,[75] where freeze–thaw cycles occur less frequently, the active layer is frozen for most of the year, much of the annual precipitation falls as snow, and when it does rain its intensity is low.[1] However, studies show that the Arctic is warming at twice the global average,[76] causing ground to freeze later and thaw earlier, the active layer to deepen,[77] and more precipitation to fall as rain.[78] This is thought to increase the frequency and rate of mass-wasting processes that remobilize sediment on Arctic hillslopes such as debris flows[69] and solifluction.[9] Hillslope–channel connectivity related to solifluction is thought to be low because of its slow movement rates (<1 mm $year^{-1}$).[10] However, solifluction monitoring sites on Svalbard have shown an increase in movement rates due to a deepening active layer caused by higher air temperatures.[9,79] In addition, regions of solifluction experience active layer detachment failures where shallow translational landslides move sedimentary material from the hillslope to adjacent channels.[80] Therefore, with solifluction being one of the most extensive landforms in our study areas, it has the potential to remobilize sediment (colluvium) locked on Arctic hillslopes.

6 | CONCLUSION

We developed a landform classification model that can be applied across Arctic mountain ranges using readily available topographic data. The model estimates the distribution of geomorphologically significant landforms using a combination of three topographic parameters: slope gradient, ERR and landscape roughness. We trained our classifier in the Endalen catchment of Svalbard, then applied the trained classifier to another Svalbard catchment (Ringdalen) and one in Alaska (Saviukviayak). The classifier is internally accurate (88.91%) when applied to landforms with strong differences in topography, such as scree slopes and solifluction sheets. Bedrock, blockfields and solifluction sheets were identified with a high degree of accuracy, with bedrock outcrops modeled at a greater resolution than was possible to map using satellite imagery. Classification accuracy did not change significantly between sites, suggesting that this method can be readily transferred between geographic locations. The process-oriented nature of our classification method allows for an improved understanding of the spatial distribution of key geomorphic processes in Arctic mountains.

ORCID

Huw Thomas Mithan https://orcid.org/0000-0002-2960-2078

REFERENCES

1. Syvitski JPM. Sediment discharge variability in Arctic rivers: implications for a warmer future. *Polar Res*. 2002;21(2):323-330. https://doi.org/10.1111/j.1751-8369.2002.tb00087.x

2. Bartsch A, Gude M, Gurney SD. Quantifying sediment transport processes in periglacial mountain environments at a catchment scale using geomorphic process units. *Geogr Ann Ser A-Physical Geogr*. 2009;91A(1):1-9. https://doi.org/10.1111/j.1468-0459.2009.00349.x

3. Bonnaventure PP, Lamoureux SF. The active layer: a conceptual review of monitoring, modelling techniques and changes in a warming climate.

Prog Phys Geogr. 2013;37(3):352-376. https://doi.org/10.1177/0309133313478314

4. Harris C, Arenson LU, Christiansen HH, et al. Permafrost and climate in Europe: monitoring and modelling thermal, geomorphological and geotechnical responses. Earth-Sci Rev. 2009;92(3–4):117-171. https://doi.org/10.1016/j.earscirev.2008.12.002

5. Harris C, Haeberli W, Vonder Muhll D, King L. Permafrost monitoring in the high mountains of Europe: the PACE project in its global context. Permafr Periglac Process. 2001;12(1):3-11. https://doi.org/10.1002/ppp.377

6. Nishimura S, Martin CJ, Jardine RJ, Fenton CH. A new approach for assessing geothermal response to climate change in permafrost regions. Geotechnique. 2009;59(3):213-227. https://doi.org/10.1680/geot.2009.59.3.213

7. Rapp A. Recent development of mountain slopes in Kärkevagge and surroundings, northern Scandinavia. Geogr Ann. 1960;42(2/3):65-200.

8. Ballantyne CK. A general model of autochthonous blockfield evolution. Permafr Periglac Process. 2010;21(4):289-300. https://doi.org/10.1002/ppp.700

9. Harris C, Kern-Luetschg M, Christiansen HH, Smith F. The role of interannual climate variability in controlling Solifluction processes, Endalen, Svalbard. Permafr Periglac Process. 2011;22(3):239-253. https://doi.org/10.1002/ppp.727

10. Matsuoka N. Solifluction rates, processes and landforms: a global review. Earth-Sci Rev. 2001;55(1–2):107-134. https://doi.org/10.1016/s0012-8252(01)00057-5

11. Hinchliffe S, Ballantyne CK, Walden J. The structure and sedimentology of relict talus, Trotternish, northern Skye, Scotland. Earth Surf Process Landforms. 1998;23(6):545-560. https://doi.org/10.1002/(sici)1096-9837(199806)23:6<545::aid-esp876>3.0.co;2-e

12. Rapp A. Talus Slopes and Mountain Walls at Tempelfjorden, Spitsbergen. A Geomorphological Study of the Denudation of Slopes in an Arctic Locality. Vol 119. Oslo: Norsk Polarinstitutt; 1960.

13. Hjort J, Ujanen J, Parviainen M, Tolgensbakk J, Etzelmüller B. Transferability of geomorphological distribution models: evaluation using solifluction features in subarctic and Arctic regions. Geomorphology. 2014;204:165-176. https://doi.org/10.1016/j.geomorph.2013.08.002

14. Romstad B, Etzelmüller B. Mean-curvature watersheds: a simple method for segmentation of a digital elevation model into terrain units. Geomorphology. 2012;139:293-302. https://doi.org/10.1016/j.geomorph.2011.10.031

15. Luoto M, Hjort J. Generalized linear modelling in periglacial studies: terrain parameters and patterned ground. Permafr Periglac Process. 2004;15(4):327-338. https://doi.org/10.1002/ppp.482

16. Marmion M, Hjort J, Thuiller W, Luoto M. Statistical consensus methods for improving predictive geomorphology maps. Comput Geosci. 2009;35(3):615-625. https://doi.org/10.1016/j.cageo.2008.02.024

17. Etzelmüller B, Odegard RS, Berthling I, Sollid JL. Terrain parameters and remote sensing data in the analysis of permafrost distribution and periglacial processes: principles and examples from southern Norway. Permafr Periglac Process. 2001;12(1):79-92. https://doi.org/10.1002/ppp384

18. Dragut L, Blaschke T, Drăguţ L, Blaschke T. Automated classification of landform elements using object-based image analysis. Geomorphology. 2006;81(3–4):330-344. https://doi.org/10.1016/j.geomorph.2006.04.013

19. Hjort J, Etzelmüller B, Tolgensbakk J. Effects of scale and data source in periglacial distribution modelling in a high Arctic environment, western Svalbard. Permafr Periglac Process. 2010;21(4):345-354. https://doi.org/10.1002/ppp.705

20. Brenning A. Benchmarking classifiers to optimally integrate terrain analysis and multispectral remote sensing in automatic rock glacier detection. Remote Sens Environ. 2009;113(1):239-247. https://doi.org/10.1016/j.rse.2008.09.005

21. Aalto J, Luoto M. Integrating climate and local factors for geomorphological distribution models. Earth Surf Process Landf. 2014;39(13):1729-1740. https://doi.org/10.1002/esp.3554

22. Giles PT, Franklin SE. An automated approach to the classification of the slope units using digital data. Geomorphology. 1998;21(3–4):251-264. https://doi.org/10.1016/s0169-555x(97)00064-0

23. Aalto J, Venalainen A, Heikkinen RK, Luoto M. Potential for extreme loss in high-latitude Earth surface processes due to climate change. Geophys Res Lett. 2014;41(11):3914-3924. https://doi.org/10.1002/2014gl060095

24. Brenning A. Spatial prediction models for landslide hazards: review, comparison and evaluation. Nat Hazards Earth Syst Sci. 2005;5(6):853-862. https://doi.org/10.5194/nhess-5-853-2005

25. Vorpahl P, Elsenbeer H, Marker M, Schroder B. How can statistical models help to determine driving factors of landslides? Ecol Model. 2012;239:27-39. https://doi.org/10.1016/j.ecolmodel.2011.12.007

26. Crouvi O, Ben-Dor E, Beyth M, Avigad D, Amit R. Quantitative mapping of arid alluvial fan surfaces using field spectrometer and hyperspectral remote sensing. Remote Sens Environ. 2006;104(1):103-117. https://doi.org/10.1016/j.rse.2006.05.004

27. Brenning A, Pena MA, Long S, Soliman A. Thermal remote sensing of ice-debris landforms using ASTER: an example from the Chilean Andes. Cryosphere. 2012;6(2):367-382. https://doi.org/10.5194/tc-6-367-2012

28. Brenning A, Long S, Fieguth P. Detecting rock glacier flow structures using Gabor filters and IKONOS imagery. Remote Sens Environ. 2012;125:227-237. https://doi.org/10.1016/j.rse.2012.07.005

29. Ju J, Roy DP. The availability of cloud-free Landsat ETM plus data over the conterminous United States and globally. Remote Sens Environ. 2008;112(3):1196-1211. https://doi.org/10.1016/j.rse.2007.08.011

30. Showstack R. Map Provides High-Resolution Look at Nearly Entire Arctic Region. Eos Earth Sp Sci News. 2017;98. https://doi.org/10.1029/2017EO085451

31. Humlum O, Instanes A, Sollid JL. Permafrost in Svalbard: a review of research history, climatic background and engineering challenges. Polar Res. 2003;22(2):191-215. https://doi.org/10.1111/j.1751-8369.2003.tb00107.x

32. Major H, Haremo P, Dallman WK, Andresen A. Geological Map of Svalbard 1:100 000, Sheet C9G Adventdalen (Revised after Major 1964); 2001.

33. Eckerstorfer M, Christiansen HH, Vogel S, Rubensdotter L. Snow cornice dynamics as a control on plateau edge erosion in Central Svalbard. Earth Surf Process Landf. 2013;38(5):466-476. https://doi.org/10.1002/esp.3292

34. Akerman HJ. Notes on talus morphology and processes in Spitsbergen. Geogr Ann Ser a-Physical Geogr. 1984;66(4):267-284. https://doi.org/10.2307/520850

35. Larsson S. Geomorphological effects on the slopes of Longyear valley, Spitsbergen, after a heavy rainstorm in July 1972. Geogr Ann Ser a-Physical Geogr. 1982;64(3–4):105-125. https://doi.org/10.2307/520639

36. Matsuoka N, Hirakawa K. Solifluction resulting from one-sided and two-sided freezing: field data from Svalbard. Polar Geosci. 2000;13:187-201.

37. de Haas T, Kleinhans MG, Carbonneau PE, Rubensdotter L, Hauber E. Surface morphology of fans in the high-Arctic periglacial environment of Svalbard: controls and processes. *Earth-Science Rev*. 2015;146:163-182. https://doi.org/10.1016/j.earscirev.2015.04.004

38. Gallant AL, Binnian EF, Omernik JM, Shasby MB. Ecoregions of Alaska. USGS Professional Paper 1567. *US Geol Surv Reston, VA*. 1995.

39. Hamilton TD. Surficial geologic map of the Noatak National Preserve, Alaska. *Prod Rep Rep Inf View this Publ USGS website Top Page Dep Nat Resour Div Geol Geophys Surv 3354 Coll Road, Fairbanks, AK 99709 Phone(907) 451–5000 Fax(907) 451–5050 C*; 2011.

40. Norwegian Polar Institute. Satellite image of Endalen and Ringdalen. NP_Ortofoto_Svalbard_WMTS_25833. © Norwegian Polar Institute.

41. Google Earth. Saviukviayak, Alaska. 68.77° N, 147.48° W, Eye altitude 6.5 km. © Landsat, Copernicus, IBCAO, SIO, NOAA, U.S. Navy, NGA, GEBCO; 2018.

42. Tolgensbakk J, Sørbel L, Høgvard K. Adventdalen, geomorphological and quaternary geological map, Svalbard 1: 100,000, Spitsbergen sheet C9Q. Nor Polarinstitutt Temakart. 2000;32.

43. Pedregosa F, Varoquaux G, Gramfort A, et al. Scikit-learn: machine learning in Python. *J Mach Learn Res*. 2011;12:2825-2830.

44. Esri R. *ArcGIS desktop: release 10*. CA: Environ Syst Res Institute; 2011.

45. Beven KJ, Kirkby MJ. A physically based, variable contributing area model of basin hydrology [un modèle à base physique de zone d'appel variable de l'hydrologie du bassin versant]. *Hydrol Sci J*. 1979;24(1):43-69.

46. Yokoyama R, Shirasawa M, Pike RJ. Visualizing topography by Openness: A new application of image processing to digital elevation models. *Photogramm Eng Remote Sensing*. 2002;68(3):257-265.

47. McKean J, Roering J. Objective landslide detection and surface morphology mapping using high-resolution airborne laser altimetry. *Geomorphology*. 2004;57(3–4):331-351. https://doi.org/10.1016/s0169-555x(03)00164-8

48. Pike RJ, Wilson SE. Elevation-relief ratio, hypsometric integral, and geomorphic area-altitude analysis. *Geol Soc Am Bull*. 1971;82(4):1079-1084.

49. Hammond EH. Small-scale continental landform maps. *Ann Assoc Am Geogr*. 1954;44(1):33-42.

50. NPI. Terrengmodell Svalbard (S0 Terrengmodell) [Data set]. 2014. https://doi.org/10.21334/npolar.2014.dce53a47. Accessed October 9, 2015.

51. USGS. 5meter Alaska Digital Elevation Model (DEM) - USGS National Map. 2015. https://www.sciencebase.gov/catalog/item/5641fe98e4b0831b7d62e758. Accessed September 2, 2016.

52. Hack JT, Goodlett JC. Geomorphology and Forest Ecology of a Mountain Region in the Central Appalachians. *Geol Survey Prof Pap*. 1960;347:66. https://doi.org/10.1016/j.msea.2005.12.083

53. Horton RE. Erosional development of streams and their drainage basins; hydrophysical approach to quantitative morphology. *Geol Soc Am Bull*. 1945;56(3):275-370.

54. Schneevoigt NJ, van der Linden S, Thamm HP, Schrott L. Detecting alpine landforms from remotely sensed imagery. A pilot study in the Bavarian Alps. *Geomorphology*. 2008;93(1–2):104-119. https://doi.org/10.1016/j.geomorph.2006.12.034

55. Clubb FJ, Mudd SM, Milodowski DT, Hurst MD, Slater LJ. Objective extraction of channel heads from high-resolution topographic data. *Water Resour Res*. 2014;50(5):4283-4304. https://doi.org/10.1002/2013wr015167

56. Passalacqua P, Do Trung T, Foufoula-Georgiou E, Sapiro G, Dietrich WE. A geometric framework for channel network extraction from lidar: Nonlinear diffusion and geodesic paths. *J Geophys Res*. 2010;115(F1). https://doi.org/10.1029/2009jf001254

57. Clubb FJ, Mudd SM, Milodowski DT, Hurst MD, Slater LJ. Geomorphometric delineation of floodplains and terraces from objectively defined topographic thresholds. *Earth Surf Dyn*. 2017;5(3):369-385.

58. Grieve SWD, Hales TC, Parker RN, Mudd SM, Clubb FJ. Controls on zero-Order Basin morphology. *Case Rep Med*. 2018;123(12):3269-3291.

59. Grieve SWD, Mudd SM, Milodowski DT, Clubb FJ, Furbish DJ. How does grid-resolution modulate the topographic expression of geomorphic processes? *Earth Surf Dyn*. 2016;4(3):627-653.

60. Gallant AL, Brown DD, Hoffer RM. Automated mapping of Hammond's landforms. *IEEE Geosci Remote Sens Lett*. 2005;2(4):384-388.

61. Minár J, Evans IS, Minar J, Evans IS. Elementary forms for land surface segmentation: the theoretical basis of terrain analysis and geomorphological mapping. *Geomorphology*. 2008;95(3–4):236-259. https://doi.org/10.1016/j.geomorph.2007.06.003

62. Jasiewicz JJ, Stepinski TF. Geomorphons – a pattern recognition approach to classification and mapping of landforms. *Geomorphology*. 2013;182:147-156. https://doi.org/10.1016/j.geomorph.2012.11.005

63. MacMillan RA, Jones RK, McNabb DH. Defining a hierarchy of spatial entities for environmental analysis and modeling using digital elevation models (DEMs). *Comput Environ Urban Syst*. 2004;28(3):175-200. https://doi.org/10.1016/S0198-9715(03)00019-X

64. Roering JJ, Marshall J, Booth AM, Mort M, Jin Q. Evidence for biotic controls on topography and soil production. *Earth Planet Sci Lett*. 2010;298(1–2):183-190. https://doi.org/10.1016/j.epsl.2010.07.040

65. Milodowski DT, Mudd SM, Mitchard ETAA. Topographic roughness as a signature of the emergence of bedrock in eroding landscapes. *Earth Surf Dyn*. 2015;3(4):483-499. https://doi.org/10.5194/esurf-3-483-2015

66. Marshall JA, Roering JJ. Diagenetic variation in the Oregon coast range: implications for rock strength, soil production, hillslope form, and landscape evolution. *J Geophys Res Surf*. 2014;119(6):1395-1417. https://doi.org/10.1002/2013jf003004

67. Salvigsen O, Nydal R. The Weichselian glaciation in Svalbard before 15,000 BP. *Boreas*. 1981;10(4):433-446.

68. Ridefelt H, Boelhouwers J, Etzelmüller B. Local variations of solifluction activity and environment in the Abisko Mountains, northern Sweden. *Earth Surf Process Landf*. 2011;36(15):2042-2053. https://doi.org/10.1002/esp.2225

69. Harris SA, Gustafson CA. Debris flow characteristics in an area of continuous permafrost, St-Elias range, Yukon Territory. *Zeitschrift Fur Geomorphol*. 1993;37(1):41-56.

70. Siewert MB, Krautblatter M, Christiansen HH, Eckerstorfer M. Arctic Rockwall retreat rates estimated using laboratory-calibrated ERT measurements of talus cones in Longyeardalen, Svalbard. *Earth Surf Process Landf*. 2012;37(14):1542-1555. https://doi.org/10.1002/esp.3297

71. Eckerstorfer M, Christiansen HH. Topographical and meteorological control on snow avalanching in the Longyearbyen area, Central Svalbard 2006-2009. *Geomorphology*. 2011;134(3–4):186-196. https://doi.org/10.1016/j.geomorph.2011.07.001

72. Harris C, Davies MCR. Gelifluction: observations from large-scale laboratory simulations. *Arct Antarct Alp Res*. 2000;32(2):202-207. https://doi.org/10.2307/1552452

73. Harris C, Davies MCR, Coutard JP. An experimental design for laboratory simulation of periglacial solifluction processes. *Earth Surf Process Landf*. 1996;21(1):67-75.

74. Heckmann T, Schwanghart W. Geomorphic coupling and sediment connectivity in an alpine catchment—exploring sediment cascades using graph theory. *Geomorphology*. 2013;182:89-103.

75. Syvitski JP, Morehead MD. Estimating river-sediment discharge to the ocean: application to the eel margin, northern California. *Mar Geol*. 1999;154(1–4):13-28.

76. Stocker TF, Qin D, Plattner GK, et al. IPCC, 2013: Summary for Policymakers in Climate Change 2013: The Physical Science Basis, Contribution of Working Group I to the Fifth Assessment Report of the Intergovernmental Panel on Climate Change; 2013.

77. Christiansen HH, Etzelmüller B, Isaksen K, et al. The thermal state of permafrost in the Nordic area during the international polar year 2007-2009. *Permafr Periglac Process*. 2010;21(2):156-181. https://doi.org/10.1002/ppp.687

78. Bintanja R, Andry O. Towards a rain-dominated Arctic. *Nat Clim Chang*. 2017;7(4):263-267. https://doi.org/10.1038/nclimate3240

79. Akerman HJ. Relations between slow slope processes and active-layer thickness 1972–2002, Kapp Linné, Svalbard. *Nor Geogr Tidsskr J Geogr*. 2005;59(2):116-128.

80. Lamoureux S, Lafreniere J, Favaro A. Erosion dynamics following localized permafrost slope disturbances. *Geophys Res Lett*. 2014;41(15):5499-5505. https://doi.org/10.1002/2014gl060677